Cerebral Cortex May 2007;17:1213-1226
doi:10.1093/cercor/bhl035
Advance Access publication July 7, 2006

GABAergic and Pyramidal Neurons of Deep Cortical Layers Directly Receive and Differently Integrate Callosal Input

Theofanis Karayannis, Icnelia Huerta-Ocampo and Marco Capogna

Medical Research Council Anatomical Neuropharmacology Unit, Department of Pharmacology, University of Oxford, Oxford OX1 3TH, UK

We studied the involvement of deep cortical layer neurons in processing callosal information in the rat. We observed with electron microscopy that both parvalbumin (PV)-labeled profiles and unlabeled dendritic spines of deep cortical layer neurons receive synapses from the contralateral hemisphere. Stimulation of callosal fibers elicited monosynaptic excitatory postsynaptic currents in both layer VI pyramidal neurons and γ-aminobutyric acidergic (GABAergic) interneurons immunopositive for the vesicular GABA transporter and PV. Pyramidal cells had intrinsic electrophysiological properties and synaptic responses with slow kinetics and a robust *N*-metyhl-D-aspartate (NMDA) component. In contrast, GABAergic interneurons had intrinsic membrane properties and synaptic responses with faster kinetics and a less pronounced NMDA component. Consistent with these results, the temporal integration of callosal input was effective over a significantly longer time window in pyramidal neurons compared with GABAergic interneurons. Interestingly, callosal stimulation did not evoke feedforward inhibition in all GABAergic interneurons and in the majority of pyramidal neurons tested. Furthermore, retrogradely labeled layer VI pyramidal neurons of the contralateral cortex responded monosynaptically to callosal stimulation, suggesting interconnectivity between callosally projecting neurons. The data show that pyramidal neurons and GABAergic interneurons of deep cortical layers receive interhemispheric information directly and have properties supporting their distinct roles.

Keywords: corpus callosum, EPSC, layer VI pyramidal cell, parvalbumin interneuron, temporal coding

Introduction

The corpus callosum is the major commissural pathway connecting the 2 cerebral hemispheres in the mammalian brain and extends widely from the frontal to the parietal lobe (Innocenti 1986). The function of this pathway has been extensively investigated at an integrative level of analysis in several mammalian species including humans, in both physiological and pathological conditions (Bogen 1986; Berlucchi and others 1995; Fabri and others 2001; Devinsky and Laff 2003; Gazzaniga 2005).

In contrast to these holistic studies, much less is known on the functional properties of the callosal-cortical circuits at a cellular level (Conti and Manzoni 1994). Neocortical pyramidal neurons, located mainly in layers II/III and V, project and form excitatory type I synapses on spines of pyramidal neurons in homo- and heterotopic areas of the contralateral cortex (Innocenti 1986). Electrophysiological recordings have been performed from pyramidal neurons of layers II/III and V in vivo or in vitro demonstrating some properties of these synaptic connections (Vogt and Gorman 1982; Hicks and Guedes 1983; Thomson 1986; Kawaguchi 1992; Kumar and Huguenard 2001, 2003; Kumar and others 2002; Cisse and others 2003, 2004), but in contrast, information on callosal input to layer VI pyramidal neurons is scant. Different from supragranular layers, pyramidal neurons of layer VI have extensive reciprocal corticothalamic connections (Beierlein and Connors 2002), which can refine thalamic spatial responses (Temereanca and Simons 2004). Therefore, direct excitation of layer VI neurons by commissural fibers would provide a novel loop for bilateral corticothalamic integration. Furthermore, layer VI pyramidal neurons also widely project to other cortical layers and areas (Zhang and Deschenes 1997, 1998), and hence, information carried by the corpus callosum would affect several other circuits (Thomson and Bannister 2003).

Parvalbumin (PV)-positive interneurons are the most numerous subtype of rat γ-aminobutyric acidergic (GABAergic) cortical interneurons (Markram and others 2004). Their activity shapes the synaptic information on cortical neurons in time and space (Gabernet and others 2005), leading to important functional consequences ranging from changes in cortical column formation (Fagiolini and others 2004) to plasticity of neuronal receptive fields (Rao and others 2000). In contrast to a wealth of information on cortical PV fast-spiking interneurons (Swadlow 2003), and although some previous studies addressed the involvement of GABAergic interneurons in the cortical-callosal network (Toyama and others 1974; Kawaguchi 1992; Kimura and Baughman 1997), the functional contribution of PV interneurons in this network has been neglected. The clarification of their role is paramount in understanding the cellular plasticity affecting the transfer of information between the cortical hemispheres.

The present work aims to elucidate novel aspects of the callosal-cortical cellular network by studying the contribution of small pyramidal neurons and GABAergic interneurons of deep cortical layers.

Materials and Methods

Slice Preparation

The data were obtained from 14- to 24-day-old Sprague–Dawley rats. The animals were deeply anesthetized using isoflurane and decapitated in accordance with procedures approved by the Home Office in line with The Animals (Scientific Procedures) Act, 1986. After decapitation, the brain was quickly removed and placed into ice-cold artificial cerebrospinal fluid (ACSF) solution (sucrose-ACSF) of composition (mM): 85 NaCl, 26 $NaHCO_3$, 2.5 KCl, 1.25 NaH_2PO_4, 2 $CaCl_2$, 2 $MgCl_2$, 10 glucose, 3 kynurenic acid, and 73.6 sucrose, saturated with 95% O_2 and 5% CO_2, at pH 7.3–7.4. The brain was glued onto the stage of a vibratome (VT 1000S, Leica Microsystems, Nussloch, Germany), and coronal slices of 300–320 μm thickness containing corpus callosum and frontal 1 and 2 cortical areas were cut. The slices were then stored at about 34 °C for at least 1 h in a submerged incubation chamber

containing sucrose-ACSF but without the kynurenic acid, which was gradually exchanged with a recording ACSF without sucrose and with 130 mM NaCl. Slices were then transferred to a recording chamber and superfused at about 33 °C at a rate of 1–2 mL/min with continuously oxygenated recording ACSF.

Electrophysiological Recordings and Data Analysis

The neurons were visually identified using a microscope (Zeiss Axioskop, Jena, Germany) with immersion differential interference contrast (DIC) objectives (× 40, × 60) coupled to an infrared (IR) camera system. Patch pipettes were pulled (Sutter Instruments Co., Novato, CA) from borosilicate glass and were filled with (mM) 126 K-gluconate, 4 KCl, 4 ATP-Mg, 0.3 GTP-Na_2, 10 Na_2-phosphocreatine, and 10 4-(2-hydroxyethyl)-1-piperazineethanesulfonic acid (HEPES), buffered to a pH of 7.3. A cesium-based intracellular solution was also used to isolate *N*-methyl-D-aspartate (NMDA) receptor–mediated excitatory postsynaptic currents (EPSCs) (NMDA-EPSCs) consisting of (in mM) 126 Cs-methansulfonate, 4 CsCl, 10 HEPES, 10 Na_2-Phosphocreatine, 4 Mg-ATP, 0.3 Na-GTP (pH 7.3 with CsOH). Biocytin (5 mg) was added to a 1 mL aliquot of intracellular solution before recording, and the final osmolarity of the intracellular solutions was 280–290 mOsm. The resistance of the electrodes was 3–6 MΩ when filled with the pipette solution, and pressure was applied. Whole-cell patch clamp recordings were performed with an EPC9/2 amplifier (HEKA Elektronik, Lambrecht, Germany) either in current clamp or in voltage clamp with a gain of 10 mV/pA. Series resistance and whole-cell capacitance was monitored during the recordings, and experiments were discontinued if series resistance increased by more than 25–30%. No correction was made for the junction potential between the pipette and the ACSF, and therefore, the recorded membrane potential, as calculated post hoc using a junction potential calculator, was 16 and 13 mV more depolarized than the true membrane potential, for K-gluconate– and Cs-methansulfonate–based intracellular solution, respectively. Extracellular stimulation rate ranging from 0.2–200 Hz was delivered by using rectangular pulses of 0.05–0.1 ms width with a concentric platinum/iridium bipolar electrode (CBARC75, FHC, Brunswick, ME) or a tungsten electrode (TM53CCINS, WPI, Sarasota, FL) connected to a constant-current isolation unit (A360, WPI). The intensity of stimulation was usually 1.5–2.5 times the minimum intensity required to evoke a response. This intensity evoked a single synaptic component in all neurons studied except in 2 cases that were not included in the analysis. The stimulation electrode was placed in the corpus callosum near the midline, location where responses were usually robust, as previously described (Kumar and Huguenard 2001). Recordings were filtered at 10 kHz and acquired online using a built-in laboratory interface (ITC-16) controlled by Pulse 8.53 software (HEKA). Analysis of intrinsic membrane properties and synaptic responses was performed using Pulse 8.53 software and IGOR Pro 4.0 software (WaveMetrics, Lake Oswego, OR). The input resistance (Rin) was calculated from the slope of steady state voltage responses to a series of current injections lasting 500 ms, whereas the fast afterhyperpolarization (AHP) was determined from the first spike in response to current injection just above threshold. The duration of the action potential was measured as the width at half amplitude between the threshold potential and the peak of the action potential, which was evoked by a strong (500–1000 pA) and short (2–4 ms) depolarizing current pulse. The membrane time constant (τ) was estimated from the monoexponential curve fitting of voltage responses to hyperpolarizing current pulses. The rectification ratio was the ratio between the steady state voltage and the peak voltage responses to hyperpolarizing current pulses. The maximal firing of the cell was determined using a current pulse of +250 pA lasting 1 s. The analysis of the α-amino-3-hydroxy-5-methyl-4-isoxazoleproprionic acid (AMPA) receptor–mediated EPSC (AMPA-EPSC) was performed as follows. The area was measured as an absolute value of the integral of the synaptic current. The latency was measured as the time between the stimulus artifact and the onset of the synaptic current. The jitter was calculated as the standard deviation of the sweep-to-sweep variation in latency within each neuron averaged over 30–50 trials. The rise time was measured as 20–80% time of the EPSC peak and the decay time by fitting with a monoexponential curve. Paired-pulse data (interstimulus interval [ISI] = 15–50 ms) were computed from the ratio of the peak amplitude of the response to the second stimulus (EPSC2) divided by the response to the first stimulus (EPSC1). Spontaneous excitatory postsynaptic currents (sEPSCs), mediated by AMPA receptors, were recorded at VH = –70 mV with a sampling rate of 10 kHz for 60 s. The recorded files were then analyzed using Minianalysis software (Synaptosoft, Decatur, GA), and values for peak amplitude, rise time (20–80%), and decay time were calculated by fitting each trace individually. Regarding the NMDA-EPSC, the rise time (20–80%) was calculated as described above for the AMPA-EPSC, whereas the decay time was obtained by fitting with a monoexponential curve the NMDA current between the peak and 100 ms after it. The peak of the average NMDA current was normalized to the AMPA-EPSC and plotted versus the holding potential (VH). In this plot, the reversal potential for the NMDA-EPSC was estimated by a line fitting the 2 normalized values closest to zero. The conductance (g) of the NMDA receptors was calculated using the equation $g = I/(V\text{H}–E\text{NMDA})$, where VH is the holding potential, ENMDA is the reversal potential of the NMDA-EPSC, and I is the peak of the synaptic current measured. For each neuron, the conductances calculated at each VH were normalized to the peak conductance (g_{max}). The latter was calculated by fitting a sigmoid Boltzmann function after plotting the conductances against VH for each neuron. Data are expressed as mean ± standard error and statistically compared by means of the test indicated throughout the text.

Histological Processing and Anatomical Evaluation

Following electrophysiological recording, slices were fixed overnight by immersion in fixative containing 4% paraformaldehyde, 0.05% glutaraldehyde, and 0.2% v/v saturated picric acid in 0.1 phosphate buffer (PB) (pH 7.4) overnight. Fixed slices were then embedded in gelatin and resectioned at 60 μm thickness. The recorded cells were labeled by avidin-biotinylated horseradish peroxidase (HRP) complex followed by peroxidase reaction using diaminobenzidine (DAB) (0.05%) as chromogen and 0.01% H_2O_2 as substrate. The sections were then dehydrated through a series of solutions of increasing concentration of ethanol and permanently mounted on slides. The axonal and dendritic patterns of the neurons were reconstructed using a drawing tube attached to a light microscope equipped with a × 100 objective. Furthermore, Nissl staining was performed by dehydrating/rehydrating the sections, immersing them in cresyl violet acetate solution (1 g in 400 mL of H_2O, pH 3.6), dehydrating, and remounting them on slides.

Immunocytochemistry

After blocking nonspecific antibody binding using 20% normal horse serum in Tris-buffered saline and 0.3% triton for 2 h, 60-μm-thick slices were incubated in streptavidin Alexa (dilution 1:300; Molecular Probes, Eugene, OR) and a rabbit antibody against vesicular γ-aminobutyric acid transporter (VGAT) (dilution 1:500; gift of Prof M. Watanabe) or mouse antibody against PV (dilution 1:5000; Swant, Bellinzona, Switzerland) for approximately 48 h at 4 °C. The slices were then washed and incubated in streptavidin Alexa (1:1000 dilution) and Cy-3–conjugated donkey anti-rabbit antibody for VGAT or Cy-3–conjugated donkey anti-mouse for PV (1:400 dilution; Jackson ImmunoResearch Laboratories, West Grove, PA) for 5–24 h. The slices were subsequently washed, mounted in Vectashield (Vector laboratories, Burlingame, CA), and viewed using a Leitz DM RB fluorescent microscope. Pictures were taken using a × 100 objective under the same microscope and displayed using dedicated software (Openlab, Improvision, Coventry, UK).

Tracer Injection

The animals were anesthetized using either a combination of hypnorm and hypnovel by an intraperitoneal injection or by inhalation of the volatile anesthetic isoflurane, and the head secured in a stereotaxic frame while maintaining the level of anesthesia with isoflurane. For retrograde labeling, in vivo pressure injection of fluorescent latex microspheres (Katz and Iarovici 1990) was performed on animals of P18–P24 postnatal age (n = 5). About 0.5–1 μL of the solution containing the microspheres was injected in retrosplenial agranular (RSA) frontal layers V–VI cortex (Paxinos and Watson 1982) and taken up by synaptic terminals residing nearby. The rats were sacrificed 1–3 days postoperatively to allow sufficient time for the beads to be transported contralaterally to the injected hemisphere. Coronal brain sections were cut from these animals, cells visualized under a rhodamine or

fluorescein filter, and recorded. Fluorescent images were obtained using a Leitz DM RB microscope with × 10 and × 40 magnification lenses.

For anterograde labeling, a P20 rat received unilateral deposits of Phaseolus vulgaris leucoagglutinin (PHAL; 2.5% in 0.1 M PB, pH 8.0; Vector Laboratories, Peterborough, UK) in RSA/frontal cortex in layers V–VI. This anterograde tracer was delivered by iontophoresis via glass micropipettes of 15-μm tip diameter using pulses (7 s on/7 s off) of cathodic positive current (5 μA) over 10 min. After a survival time of 7 days, the rats were anesthetized with ketamine (70 mg/kg) and medetomidine (0.5 mg/kg) and perfused transcardially with 50 mL of phosphate-buffered saline (PBS) (0.01 M, pH 7.4) followed by 200 mL of 0.1% glutaraldehyde and 3% paraformaldehyde in 0.1 M PB. The animals were postperfused with approximately 50 mL of PBS.

Preparation and Analysis of Tissue for Electron Microscopy

Coronal sections of both hemispheres, including the tracer injection sites, were cut on a vibrating microtome at 60 μm thickness. The sections were incubated for cryoprotection in a solution (25% sucrose, 10% glycerol) overnight then freeze thawed in isopentane (BDH Chemicals, Poole, UK) cooled in liquid nitrogen in order to increase penetration of the reagents. The sections were incubated with 1% bovine serum albumin (BSA) and 10% normal goat serum in PBS (PBS-BSA) for 2 h at room temperature. All further incubation steps were carried out in PBS-BSA containing 1% of normal goat serum. To reveal the injected and transported PHAL, sections were incubated at 4 °C for 24 h in rabbit anti-PHAL (1:1000 in PBS-BSA; Vector Laboratories), treated with goat anti-rabbit IgG (1:100 in PBS-BSA; Dako, High Wycombe, UK) overnight at 4 °C, followed by a 2-h incubation in rabbit peroxidase–antiperoxidase (1:100 in PBS-BSA; Dako) at room temperature. The bound peroxidase was then revealed with 0.025% 3,3′-diaminobenzidine using 0.006% H_2O_2 as substrate in the presence of 0.3% $NiNH_4SO_4$ (nDAB).

PV-immunoreactive structures were revealed by incubation in mouse anti-PV (1:1000 in PBS-BSA; Swant) for 24 h at 4 °C followed by biotinylated goat anti-mouse overnight (1:100 in PBS-BSA, Vector Laboratories) with the avidin-biotin-peroxidase complex method (1:100 in PBS-BSA; Vector Laboratories) for 2 h at room temperature. The peroxidase was visualized with 0.025% DAB using 0.01% H_2O_2 as substrate.

All sections were postfixed in 1% osmium tetroxide (Oxkem, Oxford, UK) in 0.1 M PB at pH 7.4 for 30 min. The sections were dehydrated through a graded series of dilutions of ethanol with 1% uranyl acetate included in the 70% ethanol solution to increase contrast in the electron microscope (EM) and infiltrated with resin overnight (Durcupan; Fluka Chemicals). They were then mounted in resin on glass microscope slides and polymerized at 60 °C for 48 h.

All sections containing the sites of injection were examined to ensure that they were correctly placed. The sections were examined under the light microscope for the PHAL tracer and PV immunoreactivity in the contralateral (RSA)/frontal cortices. PV-immunoreactive neuronal perikarya and emerging dendrites (brown reaction product) in deep cortical layers were examined at high magnification, and the positions of anterogradely PHAL-labeled terminals (black reaction product) closely apposed to them was noted, photographed digitally, and examined by correlated light and electron microscopy. The density of PHAL-labeled terminals was calculated by counting 303 putative boutons in 5 randomly selected deep cortical layer fields. The volume of the fields, measured as a cylinder, was estimated by using a calibration bar to measure their diameter and by estimating the depth up to which PV immunoreactivity could be clearly observed. The area of interest was cut from the microscope slide and re-embedded in Durcupan blocks for sectioning. Serial sections of 60–70 nm thickness were collected on Pioloform-coated single slot copper grids. The ultrathin sections were then contrasted with lead citrate for 1 min and examined in a Philips CM 10 EM.

Chemicals and Drugs

All drugs were applied to the recording preparation through the bath, unless stated otherwise. Salts used in the preparation of the intracellular recording solution and ACSF were obtained from either BDH Laboratory Supplies or Sigma (Poole, UK). The 6,7-dinitroquinoxaline-2,3-dione (DNQX), D-(-)-2-amino-5-phosphonovaleric acid (D-AP5), (-)-bicuculline methochloride, gabazine, and tetrodotoxin were purchased from Tocris Cookson (Bristol, UK).

Results

Synapses of Callosal Fibers onto Deep Cortical Layer Neuronal Profiles

We injected the anterograde tracer PHAL into deep cortical layers of the left hemisphere, and the tracer was detected as a black reaction product produced by nickel-intensified DAB. Axons labeled by PHAL in the corpus callosum crossed the midline and terminated in all layers of the homotopic area of the contralateral hemisphere. Light microscopic analysis revealed that labeled fibers had various sizes and extended with or without branching extensively, and PHAL-positive boutons were commonly observed along the axons. The second immunoreaction for the visualization of PV was detected as a brown reaction product produced by DAB alone. Somata, dendrites, and axon terminals positive for PV were found in all cortical layers in agreement with previous observations (Celio 1986). Labeling for PV showed the somata of various nonpyramidal cells, smooth and sometimes varicose dendrites, and boutons that could be clearly observed surrounding labeled and nonlabeled somata, consistent with GABAergic interneurons contacting the proximal domain of target neurons (Kawaguchi and Kubota 1997; Markram and others 2004). We searched for and found PV-positive dendrites and somata apposed by PHAL-labeled boutons in all cortical layers. Quantitatively, in deep cortical layers, 303 PHAL-labeled boutons were counted, of which 13.86% were apposed to PV-labeled elements (13.2% against dendrites and 0.66% against somata). This percentage was found similar (range: 10.60–14.92%) in all 5 randomly selected deep cortical layer regions that were analyzed, and the estimated density of the PHAL-labeled boutons was $2.46 \times 10^{-4}/\mu m^3$. It is important to note that this quantification has limitations, as the 13.86% calculated is an upper limit, because some of the boutons might make synapses with unstained structures nearby. An example of a PHAL-labeled bouton apposed to a PV-labeled dendrite in the deep layers is illustrated in Figure 1*A1*. Electron microscopic testing of this contact confirmed that the bouton indeed established a synapse with the PV-positive dendrite, as shown in Figure 1*A2,A3*. In the sample taken, 5 such commissural bouton to PV-positive dendritic synapses were observed (Fig. 1*B*), whereas one commissural bouton made a synapse with a PV-positive soma. There were numerous PV-positive boutons forming type II synapses with both PV-positive (Fig. 1*C*) and PV-negative neuronal profiles. The reaction product in the PV-positive boutons was lighter and less electron opaque than in the PHAL-labeled boutons; therefore, they could clearly be differentiated.

The postsynaptic specialization in the PV-positive neurons was covered frequently by the HRP reaction product, and therefore, its extent could not be assessed, irrespective of whether the presynaptic terminal was labeled or not. However, when the postsynaptic profile was not labeled, the extensive postsynaptic density characteristic of glutamatergic synapses made by pyramidal cell boutons was clearly visible. Several PHAL-labeled terminals were found to make synapses with nonlabeled dendritic spines of pyramidal neurons of layer VI (Fig. 1*D*, 6 synapses were identified in the sample).

These results show that callosal fibers make synapses with PV-positive interneurons and pyramidal neurons of deep cortical layers.

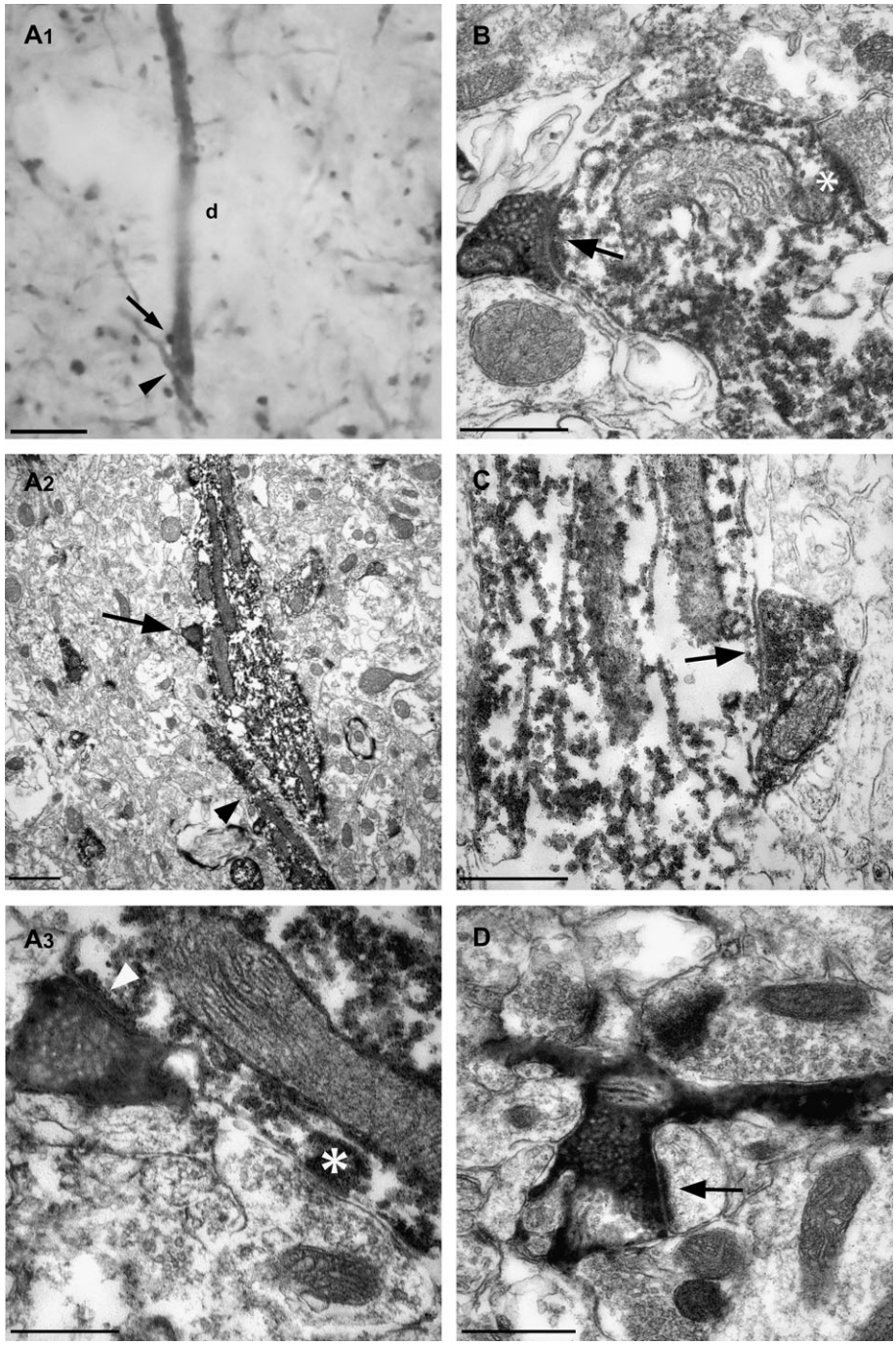

Figure 1. Commissural synaptic innervation of PV-positive neurons and pyramidal cells in the neocortex. Double immunolabeling for PHAL and PV in deep layers of Fr1/2 and RSA. (*A1*) Light micrograph of a PV-positive dendrite (d, brown in the section) closely apposed by a PHAL-positive bouton (arrow, black in the section) in the vicinity of another PV-positive dendrite (arrowhead). (*A2*) Correlated low-power electron micrograph of (*A1*) showing the closely apposed bouton (arrow) and the 2 dendrites. The arrowhead points to the same dendrite as in (*A1*). (*A3*) High-power electron micrograph of the same PHAL-labeled bouton forming a synapse (arrowhead) with the PV-positive dendrite. The same dendrite receives another synapse from an unlabeled bouton (asterisk). (*B*) Another case of a PHAL-labeled bouton that makes a synapse with a PV-positive dendrite (arrow). Note that the same dendrite receives a second synapse (asterisk) from an unlabeled bouton. (*C*) A PV-positive bouton makes a type II synapse on a PV-positive dendrite (arrow). (*D*) A PHAL-labeled axon makes a putative excitatory type I synapse onto a nonlabeled spine (arrow). Scale bars are 10 μm in (*A1*), 1 μm in (*A2*), 0.5 μm in (*A3*, *B*, *C*, and *D*).

Properties of EPSCs Evoked by Stimulation of the Corpus Callosum

Next, we addressed the properties and the functional role of the synapses identified above. To this aim, neurons were visualized under DIC-IR optics, and recordings were attempted from small layer VI pyramidal cells or putative GABAergic interneurons of deep cortical layers (layers V–VI). The recorded neurons were classified in 2 groups, namely, small pyramidal neurons (n = 60 recorded, n = 35 recovered for anatomical identification) and fast-spiking GABAergic interneurons (n = 45 recorded, n = 30 recovered for anatomical identification), based on electrophysiological and anatomical characterization. Cortical layers were identified during the recordings and confirmed by Nissl staining.

The first group of neurons (layer VI pyramidal neurons, resting membrane potential [*V*rm] = –63.4 ± 1.4 mV, n = 31) exhibited EPSCs with a mean peak amplitude of 40.7 ± 5.5 pA (*V*H = –65 mV, n = 31, Fig. 2*A*, Table 1), which were abolished by DNQX (40 μM), and were thus mediated by AMPA receptors. The EPSCs were evoked without failures in 19 neurons, whereas a few failures (range: 3–30%) were present in the other 12 cells. They were characterized by relatively slow kinetics, and their decay was well fitted with a monoexponential function. The EPSCs could follow repetitive stimulation at theta (10 Hz) and gamma frequency (40 Hz), and virtually all showed short-term depression. The mean standard deviation of the latencies (jitter) of individual traces was 0.21 ± 0.02 ms (n = 31). Thus, the low jitter values, which did not change by increasing the stimulation intensity, together with the ability of the EPSCs to follow high-frequency stimulation and the low failure rate suggest a monosynaptic origin. The pyramidal cells displayed relatively high *R*in, large membrane τ, average spike half width close to 1 ms, and action potentials that moderately adapted when stimulated with long-lasting depolarizing current pulses (Fig. 2*B*, Table 2).

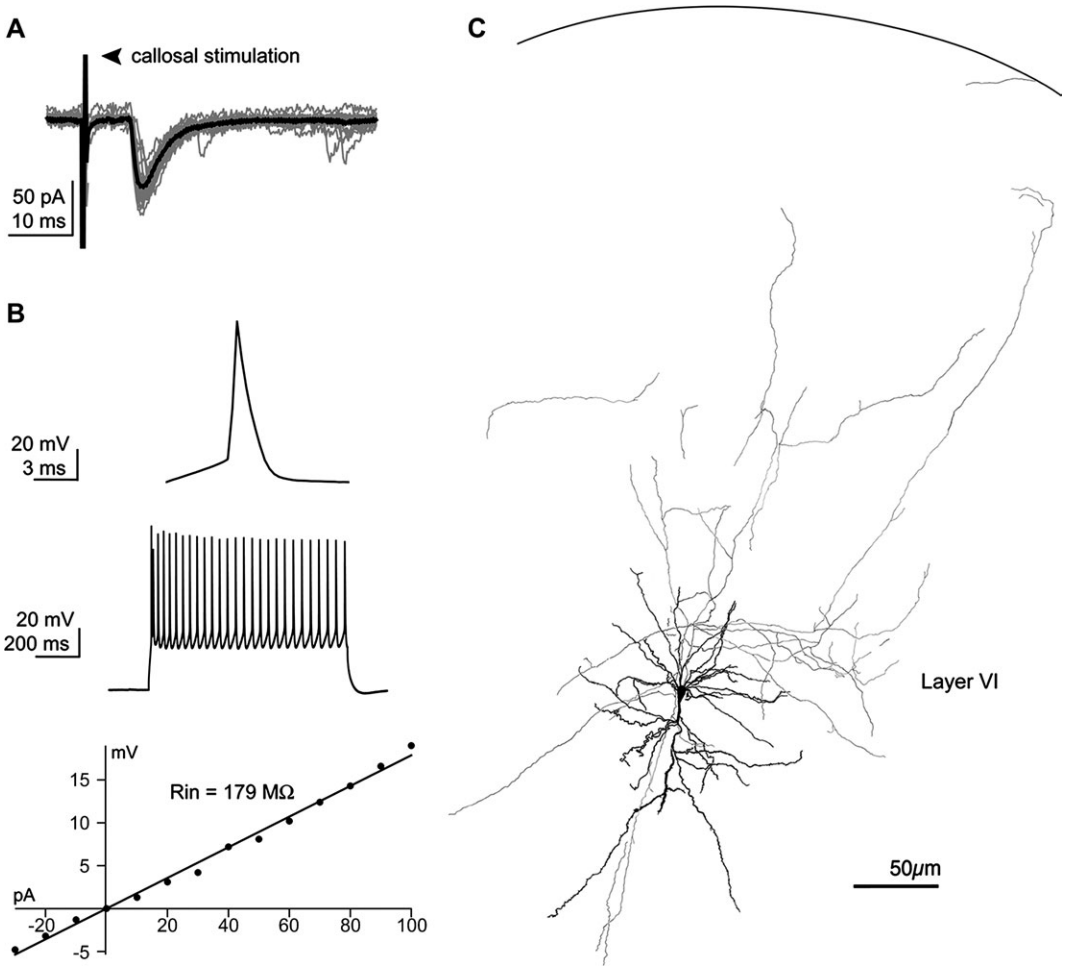

Figure 2. Layer VI pyramidal neuron of the RSA/frontal cortex responds to callosal stimulation. (*A*) The monosynaptic EPSCs recorded in this neuron in voltage clamp after stimulation of the corpus callosum (artifact). The black trace is the average of 30 sweeps (gray traces). In this cell, rise time was 0.67 ms, decay time constant was 3.8 ms, latency was 7.4 ms, jitter was 0.13 ms, and failure rate was 0%. (*B*) Electrophysiological properties of the same neuron illustrating an action potential of moderate width evoked by a depolarizing current pulse and sustained firing pattern in response to a longer current stimulus. The I/V plot used to measure *R*in is also shown. (*C*) Reconstruction using camera lucida (× 100) of the pyramidal neuron recorded, dendrites (black), and axon (gray). The cell is a layer VI small inverted pyramidal neuron with the spiny apical dendrite oriented toward the white matter and the axon running parallel to it giving off branches in several cortical layers.

Table 1
Synaptic properties of GABAergic interneurons and pyramidal cells of deep cortical layers

	Age (days)	Rise time (ms)	Decay (ms)	Area (fC)	Peak amplitude (pA)	Latency (ms)	Jitter (ms)	Failure rate (%)	PPR	10 Hz	40 Hz
GABAergic interneurons (n = 19)	21.3 ± 1.3	***0.66 ± 0.13	***2.68 ± 0.27	279.8 ± 35.9	**75.2 ± 10.2	6.3 ± 0.2	0.22 ± 0.02	4.8 ± 2.5	0.87 ± 0.1	Depress	Depress
Pyramidal cells (n = 31)	19 ± 0.6	1.24 ± 0.15	7.11 ± 0.93	310.5 ± 36.3	40.7 ± 5.5	6.8 ± 0.3	0.21 ± 0.02	5.1 ± 1.4	1 ± 0.05	Depress	Depress

Note: All values are shown as mean ± standard error of mean. Comparison between the properties of interneurons and pyramidal cells (**P < 0.01, ***P < 0.001; Mann–Whitney test).
PPR, paired pulse ratio.

The neurons displayed heterogeneous axonal and dendritic patterns observed with light microscopy; however, we could divide them in 2 subgroups. The neurons of the first subgroup (45%) were layer VI small inverted pyramidal neurons (van Brederode and Snyder 1992) with the spiny apical dendrite oriented toward the deep cortical layers almost reaching the callosal fibers and the axon running parallel to it giving off several branches (Fig. 2*C*). The second subgroup (55%) consisted of upright layer VI small pyramidal neurons with an apical dendrite with spiny branches and axon reaching the superficial cortical layers (not shown). When immunoreactivity for VGAT, a specific marker for GABAergic neurons, was performed, none of these cells were positive (not shown, $n = 4$).

The second group of neurons consisted of fast-spiking interneurons recorded in deep cortical layers of the RSA/frontal cortex (*V*rm = –69.8 ± 1.6 mV, $n = 19$). Callosal stimulation evoked EPSCs with a single peak (Fig. 3*A*, Table 1), having a mean peak amplitude of 75.2 ± 10.2 pA. Moreover, EPSCs with 2 peaks were also detected ($n = 2$), but these cells were not included in the analysis. The EPSCs had fast kinetics in terms of their rise time (0.66 ± 0.13 ms, $n = 19$) and decay (2.68 ± 0.27 ms, $n = 19$). Failures were observed only in 3 neurons (range: 3–35%), and the jitter was always small (0.22 ± 0.02 ms, $n = 19$). Synaptic depression was observed in the majority of neurons stimulated with theta (10 Hz) or gamma (40 Hz) frequency ($n =$ 6 and 7, respectively), whereas either facilitatory or steady EPSCs during the stimulation were observed in a minority of neurons ($n = 3$). The low jitter values, which did not change by enhancing the stimulation intensity, the ability of the EPSCs to follow high-frequency stimulation, and the low failure rate indicate that the EPSCs were monosynaptic. Accordingly, when we decreased the extracellular Ca^{2+} and Mg^{2+} ratio and hence the release probability, the paired-pulse ratio was increased and the amplitude of the first EPSC was decreased without affecting its latency (not shown). The interneurons were characterized by low *R*in, small membrane τ, fast spikes, and nonadapting firing pattern when stimulated with a 1-s-long depolarizing current pulse (Fig. 3*B*, Table 2). The reconstruction of a representative interneuron is illustrated in Figure 3*C*. The neurons had multipolar somata with aspiny dendrites and an axon profusely branching with a pattern typical of cortical basket cells. Moreover, VGAT and PV immunoreactivity was clearly observed in 100% (Fig. 3*D*, $n = 4$) and 90% (Fig. 3*E*, $n = 10$) of neurons tested, respectively.

When the data of passive and active membrane properties as well as synaptic responses recorded in pyramidal neurons and GABAergic interneurons were compared statistically, several differences emerged (Table 1 and 2).

These data, taken together, indicate that small pyramids of layer VI and GABAergic interneurons of deep cortical layers are excited monosynaptically by the callosal input that has different synaptic kinetics.

Is the Different EPSC Kinetics Synapse Specific?

To address this issue, we compared spontaneous AMPA-EPSCs (sEPSCs, abolished by 20 μM DNQX) originating from heterogeneous cortical synapses onto the 2 groups of neurons. The events recorded from GABAergic interneurons displayed distributions with shorter rise time and decay and higher peak amplitude and frequency than pyramidal neurons (Kolmogorov–Smirnov test, $P < 0.0001$, $n = 4$ each group, Fig. 4). The mean values for rise time, decay, and peak amplitude in pyramidal cells and interneurons, respectively, were 1.18 ± 0.03 and 0.65 ± 0.02 ms, 4.36 ± 0.15 and 2.29 ± 0.05 ms, and 15.4 ± 0.3 and 28.3 ± 0.77 pA. Interestingly, we observed only a weak correlation between the rise time and the decay of sEPSCs in both groups ($r = 0.35$ in pyramidal cells and $r = 0.39$ in interneurons). These data, taken together, suggest that the receptor subtypes and not intrinsic membrane properties present at specific cell types are likely to determine the kinetic differences observed in the callosally evoked EPSCs.

Cell-Specific Differences in the NMDA Receptor–Mediated Component of the EPSCs

Next, we investigated whether NMDA-EPSCs evoked by callosal stimulation were present and differed between pyramids and interneurons of deep cortical neurons. By using a Cs-based intracellular pipette solution to block K^+ channels and $GABA_B$ receptors, we changed the membrane potential of the recorded neurons gradually from –65 to +40 to study the NMDA-EPSC at various *V*H (Fig. 5*A*). These experiments were performed in the presence of gabazine (4 μM) and DNQX (20 μM) to block $GABA_A$ and AMPA receptors, respectively. The neurons tested were anatomically recovered and identified either as pyramidal cells ($n = 8$ out of 8) or interneurons ($n = 6$ out of 8) also in this series of experiments. When the peak amplitude of the NMDA-EPSCs was normalized to the AMPA-EPSCs recorded before the application of gabazine and DNQX for each recording, to account for cell variability, interneurons exhibited smaller values compared with pyramidal cells at several *V*H (Fig. 5*B1*, $P < 0.05$, Mann–Whitney test). In order to compare the voltage dependency of the conductance of the NMDA receptors and indirectly the receptor subunit composition in the 2 groups of neurons, the conductance was calculated at various *V*H and normalized to the peak NMDA-EPSC conductance. We constructed g/g_{max}-V plots and fitted with a sigmoid function to

Table 2
Intrinsic membrane properties of GABAergic interneurons and pyramidal cells of deep cortical layers

	Age (days)	*V*rm (mV)	*R*in (MΩ)	τ (ms)	*C*m (nF)	Sag ratio	AP width (ms)	AP amplitude (mV)	Fast AHP (mV)	Adaptation index	Maximum firing
GABAergic interneurons (n =19)	21.3 ± 1.3	**−69.8 ± 1.6	**162.8 ± 18.7	***11.9 ± 1.4	***0.10 ± 0.03	*0.97 ± 0.01	***0.42 ± 0.06	*104.1 ± 3.4	*18.9 ± 1.1	***0.68 ± 0.04	***118.2 ± 14.6
Pyramidal cells (n =31)	19 ± 0.6	−63.5 ± 1.4	263.9 ± 22.5	30 ± 1.6	0.13 ± 0.01	0.91 ± 0.01	0.98 ± 0.06	113.1 ± 2.9	15.2 ± 0.6	0.35 ± 0.02	22.2 ± 2.1

Note: All values are shown as mean ± standard error of mean. Comparison between the properties of interneurons and pyramidal cells (*$P < 0.05$, **$P < 0.01$, ***$P < 0.001$; Mann–Whitney test). *C*m, membrane capacitance; AP, action potential.

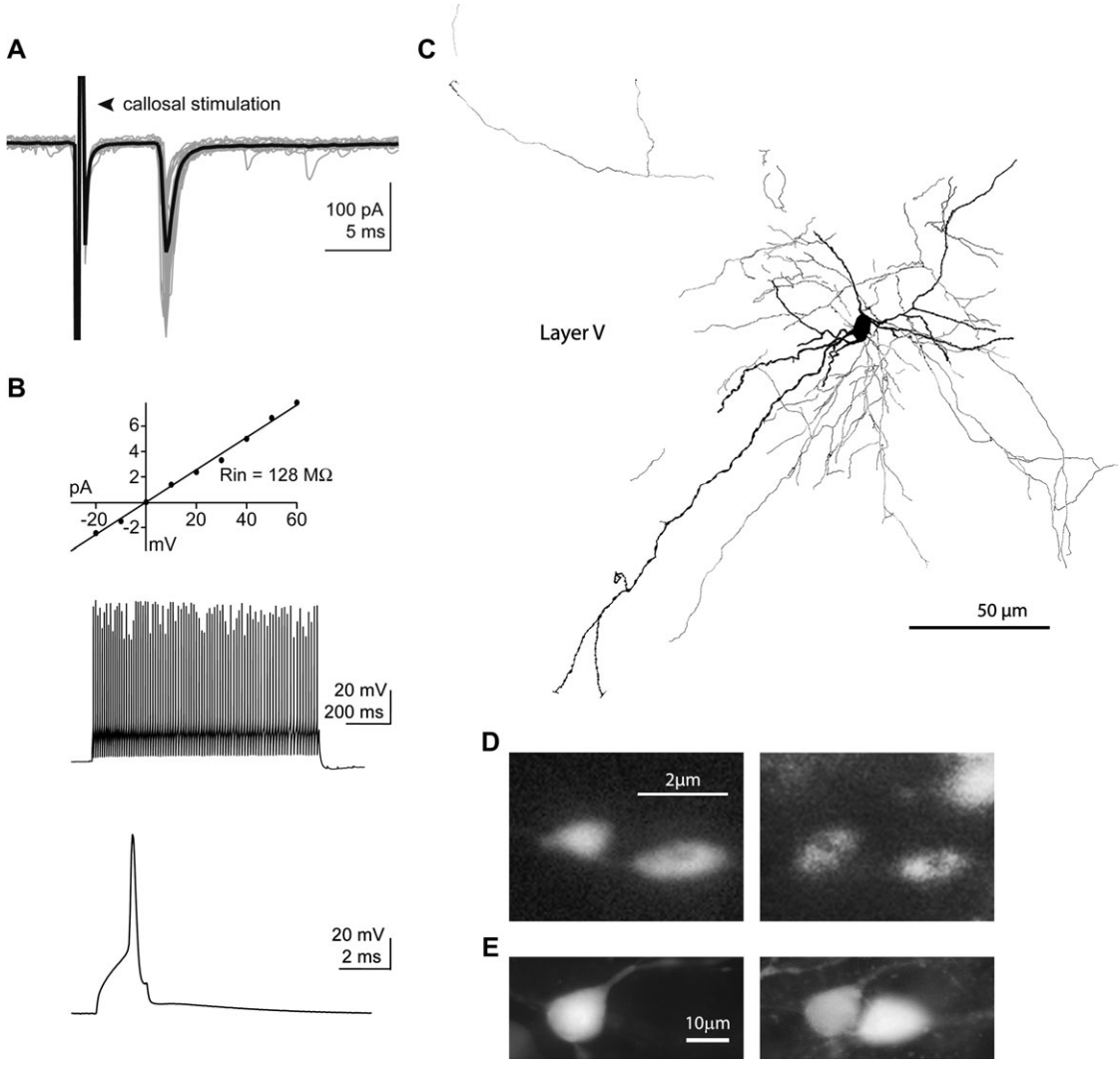

Figure 3. A deep cortical layer GABAergic interneuron of the RSA/frontal cortex responds to callosal stimulation. (*A*) The monosynaptic EPSCs recorded in this neuron in voltage clamp elicited by stimulation of the corpus callosum (artifact). The black trace is the average of 30 sweeps (gray traces). In this cell, rise time was 0.27 ms, decay time constant was 0.67 ms, latency was 6.2 ms, jitter was 0.15 ms, and failure rate was 0%. (*B*) Electrophysiological properties of the same neuron showing fast- and nonadapting firing. The I/V plot used to measure *R*in is also illustrated. (*C*) Camera lucida reconstruction (× 100) of the interneuron recorded, dendrites (black), and axon (gray). We identified this neuron as a basket cell, due to its multipolar soma with a spiny dendrites and an axon profusely but locally branching with varicosities distributed along the axonal branches contacting cell somata in a typical punctuated pattern. (*D*) VGAT immunopositive boutons (right picture) of a biocytin-filled cell (left picture) with similar features as above imaged with a fluorescent microscope with a × 100 objective. (*E*) PV immunopositivity (right picture) of a biocytin-filled neuron (left picture); another PV-positive soma is also shown (right picture).

estimate the potential at which g/g_{max} was 0.5 (*V*half). No significant difference was found between the 2 groups (Fig. 5*B2*, $P > 0.05$, Mann–Whitney test). Likewise, the estimated mean reversal potential of the NMDA-EPSCs was 9.4 ± 1.5 mV in pyramidal cells and 6.1 ± 3.4 mV in interneurons, and these values were not significantly different ($P > 0.05$, Mann–Whitney test, $n = 8$ for each, Fig. 5*C2*). On the other hand, the decay of the NMDA-EPSCs recorded at + 40 mV was significantly faster in interneurons compared with pyramidal cells (34.25 ± 5.81 and 76.63 ± 18.16 ms, respectively, Fig. 5*C1*, $P < 0.05$, Mann–Whitney test), whereas the rise time was not different (3.04 ± 0.49 ms for interneurons and 3.23 ± 0.36 ms for pyramidal cells, $n = 8$ each, $P > 0.05$, Mann–Whitney test). The detection of NMDA-EPSCs in the presence of the AMPA receptor antagonist further confirmed that the callosally evoked responses were monosynaptic and not due to intercalated excitatory cells (Mori and others 2004). Interestingly, the jitter of the NMDA-EPSCs (0.22 ± 0.02 ms, $n = 16$) was similar to that described above for the AMPA-EPSCs recorded with K-gluconate, further suggesting the monosynaptic nature of the latter. These results indicate that the NMDA component of the synaptic response evoked by callosal stimulation is less pronounced and prolonged in interneurons than pyramidal cells.

Feedforward Inhibition Triggered by Callosal Fibers

Synaptic excitation is usually curtailed by feedforward inhibition, which in this way regulates the temporal integration of excitatory inputs (Gabernet and others 2005). Therefore, we addressed whether feedforward inhibition in pyramidal neurons and GABAergic interneurons of deep cortical layers was present after callosal stimulation. For this purpose, neurons were studied in voltage clamp at –50 mV, which is a potential away from E_{GABA}, to disclose the presence of a synaptically evoked inhibitory response. Surprisingly, we did not observe any outward

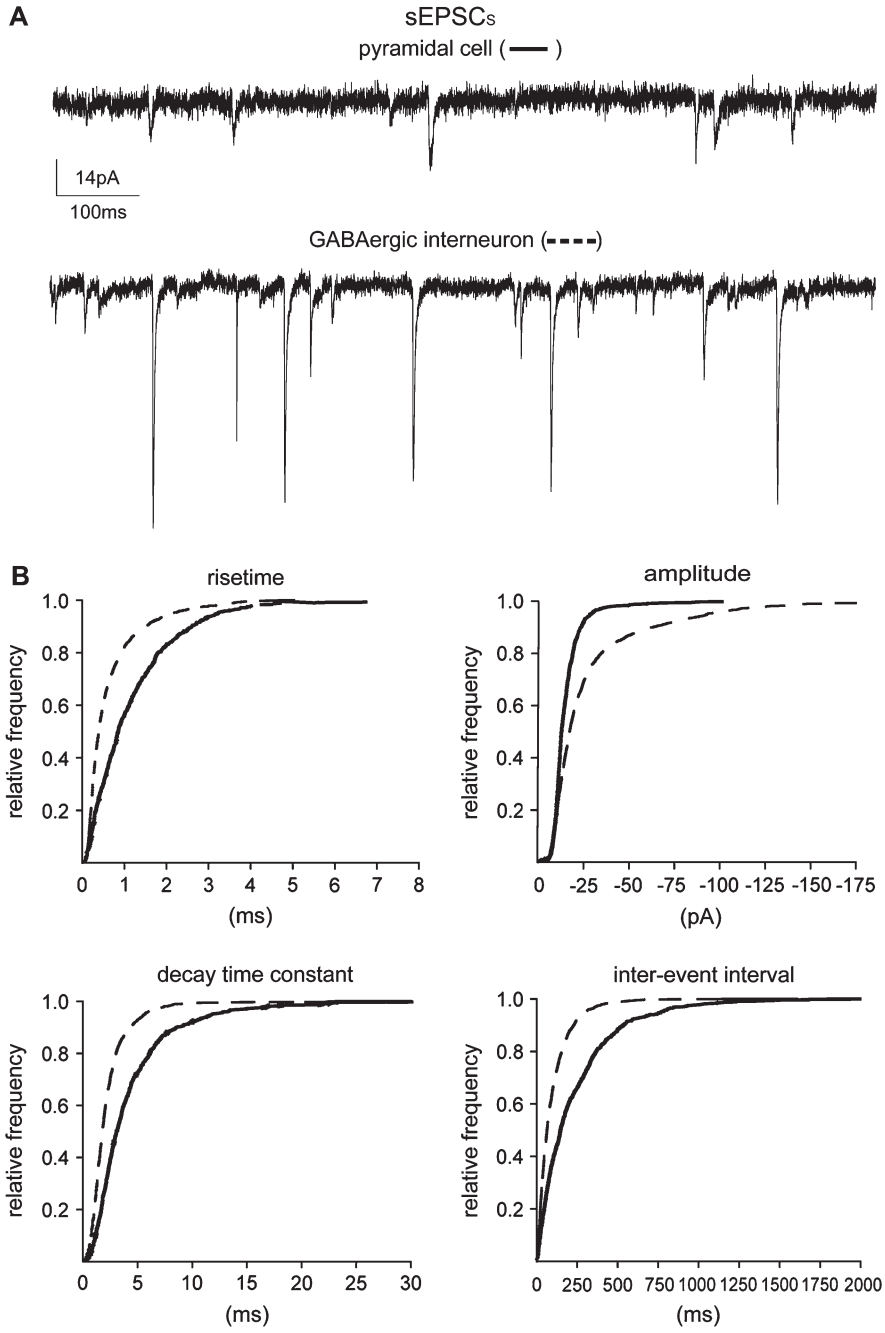

Figure 4. Different properties of sEPSCs recorded in pyramidal cells and interneurons responding to callosal stimulation. (*A*) Representative traces of sEPSCs recorded in a pyramidal cell and in a GABAergic interneuron. (*B*) Cumulative plots of pooled data of 20–80% rise time, peak amplitude, decay time constant, and interevent interval of sEPSCs recorded from pyramidal ($n = 4$) and GABAergic neurons ($n = 4$). Each comparison is statistically significant ($P < 0.0001$, Kolmogorov–Smirnov test). The number of events analyzed was 840 and 1979 for 20–80% rise time, peak amplitude, decay time constant, and 1024 and 2448 for interevent interval in pyramidal cells and interneurons, respectively.

current following the EPSCs when recording from the majority of pyramidal neurons (Fig. 6*A*, $n = 44$ out of 51) or in all interneurons studied ($n = 21$, Fig. 6*C1*), whereas a minority of pyramidal neurons displayed an outward current (Fig. 6*B*). In order to test this further, neurons were subjected to high-frequency stimulation (up to 40 Hz in voltage clamp and up to 200 Hz in current clamp) at further depolarized membrane potential (VH = –40 mV and about 10 mV below the action potential membrane threshold, respectively), to induce temporal summation of the excitatory postsynaptic potentials (EPSPs) in intercalated GABAergic neurons and to increase the driving force for inhibitory events in the recorded cells, respectively. In these experiments, inhibitory postsynaptic currents (IPSCs) or inhibitory postsynaptic potentials (IPSPs) were detected only in some but not all pyramidal neurons and never seen in interneurons (not shown, but see also Fig. 7*A1*). When IPSCs were detected they were polysynaptic because they were abolished by application of DNQX and D-AP5 (40 μM each, Fig. 6*B*). In the cases where IPSCs were detected, these neurons were not included in the EPSC kinetic analysis to avoid any contamination by the IPSCs. It is worth to mention that outward spontaneous IPSCs were detected, albeit at a low rate, in the

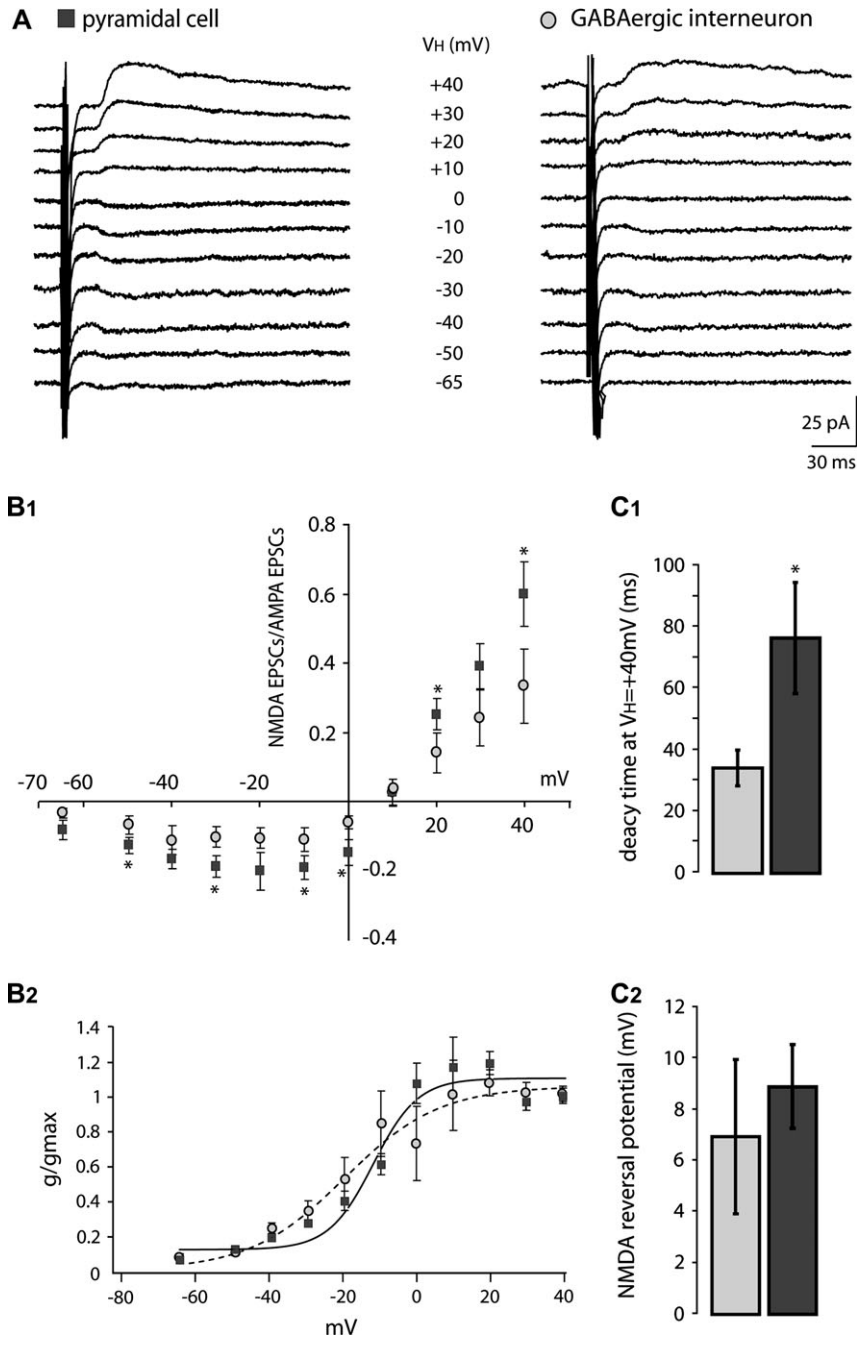

Figure 5. Different properties of NMDA-EPSCs evoked by callosal stimulation and recorded in pyramidal neurons and interneurons. (*A*) NMDA receptor–mediated synaptic currents elicited by callosal stimulation at several *V*H in the presence of gabazine (4 μM) and DNQX (20 μM) recorded from a pyramidal cell and a GABAergic interneuron. (*B1*) Plot of the peak amplitude of NMDA-EPSCs normalized to AMPA-EPSC peak amplitude against *V*H with the standard error indicated. (*B2*) Graph of pooled normalized *g–V* data superimposed with Boltzmann curve. Pooled data of the decay time (*C1*) and the reversal potential (*C2*) of the NMDA-EPSC in the 2 groups of neurons. For each graph, 8 pyramids and 8 interneurons were analyzed. For all graphs, * denotes $P < 0.05$ with Mann–Whitney test.

neurons recorded at –50 mV (Fig. 6*C2*). Therefore, callosal fibers appear to trigger feedforward inhibition only in a subset of layer VI pyramids but not onto interneurons of deep cortical layers.

Temporal Integration of Callosally Evoked Responses Is Different between Pyramidal Cells and GABAergic Interneurons

All the data presented so far suggest that layer VI pyramidal cells and interneurons are likely to integrate the callosal input within a different temporal time window. This issue was addressed with experiments where the neurons were recorded in current clamp and repetitive callosal stimulation was employed. In these experiments, the membrane potential was kept at about 10–15 mV below the action potential threshold for each cell and only the cells without feedforward inhibition were used (see above). Under these conditions, 4 callosal stimuli delivered at 40–200 Hz produced temporal summation of evoked EPSPs. When pyramidal cells were recorded ($n = 9$), the probability to elicit an action potential riding on EPSPs was inversely correlated with increasing ISIs (Fig. 7*A1*). Importantly, even at gamma

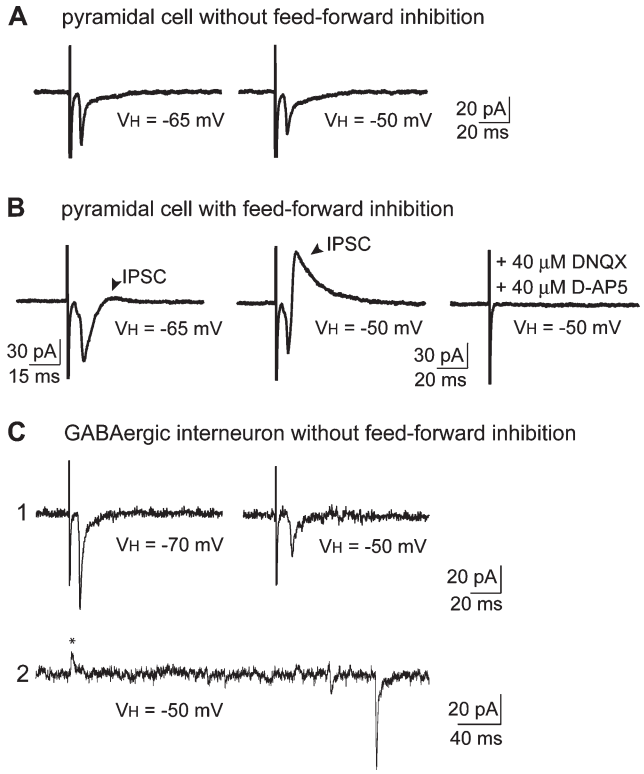

Figure 6. Presence or absence of feedforward inhibition evoked by stimulation of the corpus callosum in pyramidal cells and interneurons. Voltage clamp recording of 2 pyramidal neurons (*A, B*) and an interneuron (*C1*) after callosal stimulation at different *V*H. The stimulation evoked only EPSCs in *A, C*, but also an IPSC in *B*, where all synaptic currents were subsequently abolished by DNQX and D-AP5. (*C2*) A representative trace of spontaneous synaptic currents showing an outward IPSC (asterisk) recorded in the GABAergic interneuron.

frequencies, the stimulation could trigger action potentials. When interneurons were recorded ($n = 8$), a similar correlation was observed but shifted toward significantly lower ISI (Fig. 7*A2*, $P < 0.05$, *t*-test and Mann–Whitney test). NMDA receptors should be activated at the depolarized membrane potential and could contribute to the integration of the EPSPs. This was tested with 5-ms ISI that was associated with the highest occurrence of action potentials. Application of 40 μM D-AP5 reduced the likelihood of action potential occurrence in both groups of neurons, albeit at a significantly less extent in GABAergic interneurons, consistent with our finding that GABAergic interneurons had less pronounced NMDA-EPSCs (Fig. 7*B1,B2*).

These results demonstrate that pyramidal neurons integrate the callosal information over a longer time window than interneurons.

Are Neurons of Layer VI Interconnected via the Callosal Fibers?

To investigate this issue, we performed in vivo pressure injection of fluorescent microspheres into deep cortical layers of RSA/frontal cortex ($n = 5$ rats). After 1–3 days, this resulted in fluorescent positive cells in the contralateral hemisphere. Virtually all labeled cells appeared to have pyramidal shape, including those with the soma in layer VI (Fig. 8*A*). Labeled neurons in layer VI were then patched and after histological processing were identified either as small inverted or upright pyramidal neurons (Fig. 8*B,C*, $n = 7$). In these cells, callosal stimulation evoked EPSCs recorded in voltage clamp at –65 mV ($n = 6$, Fig. 8*B*). These EPSCs had similar kinetics and jitter values to the callosally evoked EPSCs in our previously described pyramidal cells, consistent with their monosynaptic nature, and they also lacked feedforward inhibition when tested at more depolarized *V*H. In only one case, no evoked EPSCs were detected, but, interestingly, an outward current was observed upon depolarization to –50 mV, blocked by 20 μM DNQX, consistent with a polysynaptic response. Thus, the same layer VI pyramidal neurons that send their axon contralaterally also receive a monosynaptic input from callosal fibers.

Discussion

We provide here evidence for the presence of synapses between callosally projecting neurons and anatomically identified layer VI pyramidal cells and GABAergic interneurons of deep cortical layers. The properties of the synapses were different, conferring a longer time window for integration of the callosal input to pyramidal neurons than GABAergic interneurons.

Factors Determining the Integrative Properties of the Neurons Studied

The intrinsic electrophysiological properties of the pyramidal neurons and the GABAergic interneurons studied were different. The membrane τ and the *R*in were smaller in interneurons compared with pyramidal cells, so that a given input would result in a faster and smaller response in the former cell type. Furthermore, in contrast to pyramidal neurons, interneurons had fast action potentials followed by fast and pronounced AHPs and were able to sustain firing upon depolarization with little adaptation. Consistent with the differences in basic electrophysiological properties, the kinetics of evoked AMPA-EPSC and sEPSCs were slower in pyramidal cells than in interneurons, as shown in other central synapses (Hestrin 1993; Jonas and others 1993; Geiger and others 1997; Povysheva and others 2006). The EPSC time course depends on several parameters including the time course of the presynaptic release and the clearance of glutamate from the synaptic cleft, the gating, and subunit composition of AMPA receptors (Jonas 2000), as well as the membrane time constant and the presence/absence of dendritic spines of the postsynaptic neuron (Tsay and Yuste 2004). Because sEPSCs showed kinetic differences between the 2 groups of cells and no correlation was detected between rise time and decay within the same group, the kinetic differences of the callosally evoked EPSCs were likely due to differences in AMPA receptor subtypes, to a lesser extent in time constants and not input specific (Hestrin 1993). It is unlikely that the different kinetics of the evoked AMPA-EPSCs of the 2 groups are caused by an overt different number of presynaptic fibers stimulated because we observed similar differences also in sEPSCs kinetics. In this respect, our data fully agree with a recent study that found similar kinetic differences in EPSCs whether evoked by stimulation of several fibers, by minimal stimulation, or when comparing miniature events recorded from layer II/III rat cortical pyramidal neurons and fast spiking (FS) interneurons (Povysheva and others 2006). We also observed that the frequency and amplitude of AMPA-sEPSCs were higher in interneurons than pyramidal cells. This high level of synaptic background contributes to the behavior of interneurons as coincidence detectors (Angulo and others

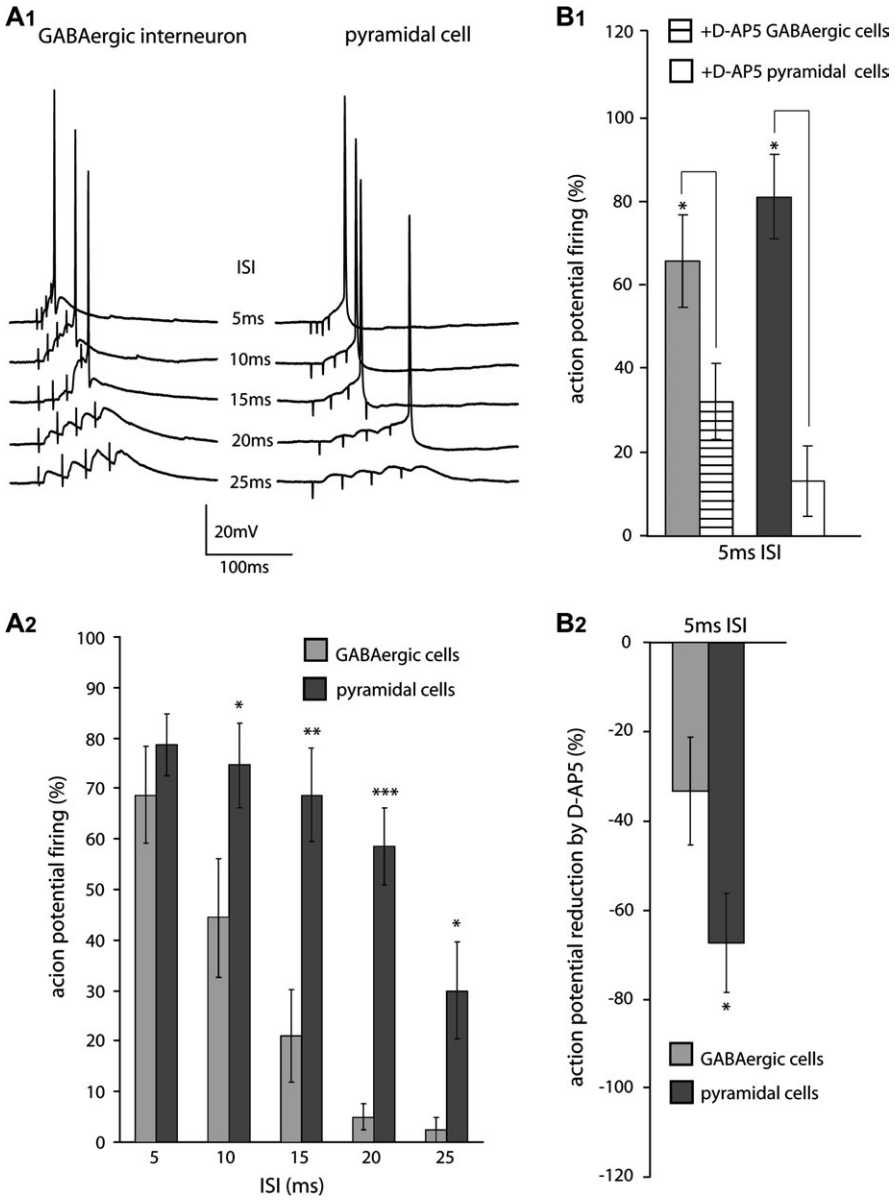

Figure 7. Different temporal integration of synaptic responses evoked by callosal stimulation in pyramidal neurons and interneurons. (*A1*) Representative current clamp recordings (single sweeps) showing EPSPs evoked by 4 stimuli at different frequencies in a pyramidal cell and a GABAergic interneuron. (*A2*) Pooled data illustrate the different percentage of action potential firing after callosal stimulation at different ISI in the 2 groups of neurons. (*B1*) Pooled data showing the reduction in the likelihood of action potential occurrence by D-AP5 (40 μM) and its differential effect between the 2 groups of cells (*B2*). In the histograms, * denotes $P < 0.05$, ** $P < 0.01$, *** $P < 0.001$ with Mann–Whitney test (*A2*, *B2*) and Wilkoxon signed rank test (*B1*).

1999) because inputs will be shunted unless they arrive within a narrow time window.

The NMDA-EPSCs were also different in the pyramidal cells compared with interneurons. In 3 interneurons, these currents were undetectable or minimal, in agreement with a similar lack of NMDA-EPSCs in interneurons of hippocampal stratum radiatum (Sah and others 1990) and with low or undetectable levels of the NR1 subunit of the NMDA receptor in PV-positive GABAergic interneurons of the same hippocampal layer (Nyiri and others 2003). The decay of the NMDA-EPSCs was slower in pyramidal cells compared with interneurons. The rise time, the reversal potential of the NMDA-EPSC, and the voltage dependency of the NMDA conductance were not significantly different between the 2 groups of neurons, suggesting indirectly that the subunit composition of the NMDA receptor may not differ. Therefore, we suggest that the differences observed in the NMDA-EPSCs are better explained by the different intrinsic membrane properties of the recorded neurons and not by heterogeneity of NMDA receptors expressed in the pyramids versus interneurons. Interestingly, NMDA receptor–mediated responses elicited by callosal stimulation have been previously detected in layer II/III or V pyramidal cells with large soma size (Thomson 1986; Kumar and Huguenard 2003) and were similar to those we report here in layer VI pyramidal cells.

The EPSCs studied were monosynaptic as the synaptic jitter of both AMPA-EPSC and NMDA-EPSC was short and independent from the stimulation intensity, the AMPA-EPSCs followed high-frequency stimulation with small failure rate and were

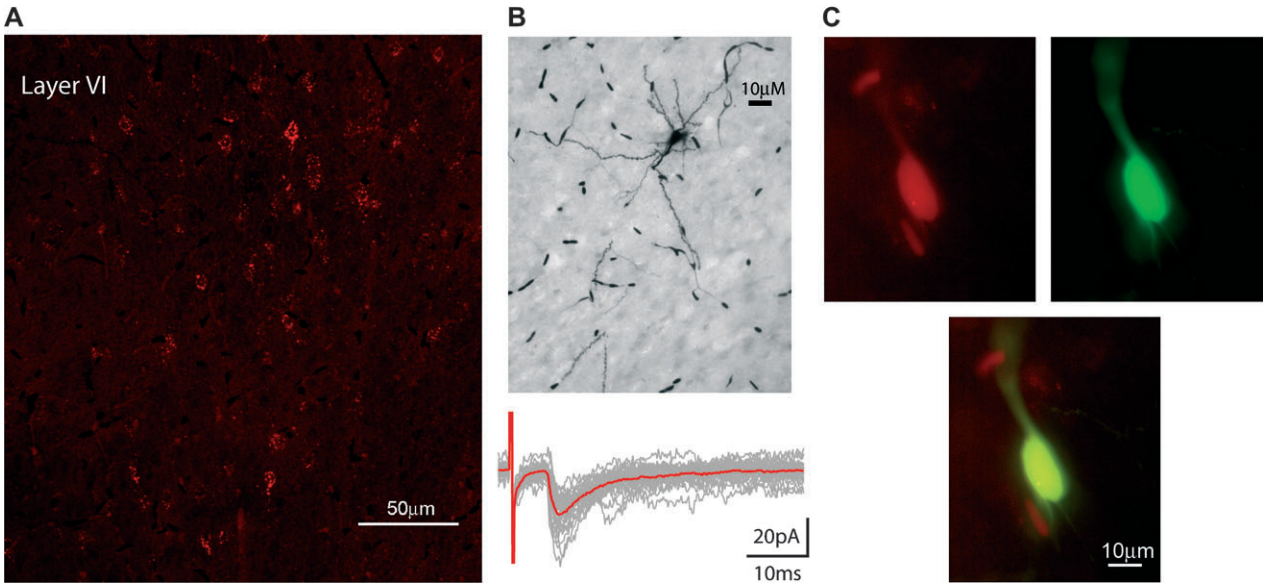

Figure 8. Layer VI pyramidal neurons of the 2 hemispheres are reciprocally connected. (*A*) Image of layer VI retrogradely labeled cells in RSA/frontal cortex after injection of fluorescent latex microspheres in the homotopic area of the contralateral hemisphere. (*B*) A retrogradely (not shown) and biocytin-labeled inverted pyramid of layer VI. This neuron responded to callosal stimulation with EPSCs (red trace, average; gray traces, 30 individual sweeps). (*C*) High magnification image of an upright layer VI pyramidal neuron double labeled with the latex microspheres (red) and biocytin (green) (yellow, merged picture) that also responded to the callosal stimulation (not shown).

resistant to low-release probability. These parameters are reliable indicators of monosynaptic responses (Doyle and Andresen 2001; Mori and others 2004). Moreover, it is unlikely that the excitatory responses recorded were elicited by back-propagated action potentials traveling along axon collaterals of callosally projecting pyramidal cells located ipsilaterally to the recorded neurons. This would go against our finding that injection of the anterograde tracer PHAL resulted in labeled boutons that make synapses on PV-positive profiles and on dendritic spines of deep cortical layers of the contralateral hemisphere. Furthermore, collaterals from callosal axons occur much more frequently in superficial than deep cortical layers (White and Czeiger 1991), consistent with the low probability to get synaptically coupled pairs of layer VI corticothalamic pyramidal neurons (West and others 2006), which represent 55% of our pyramidal cell sample.

Given the importance of feedforward inhibition pathways in modulating the integration of neuronal responses (Buzsaki 1984; Gabernet and others 2005), we searched for feedforward inhibition in our experiments. Surprisingly, we found that only some pyramidal cells and none of the GABAergic interneurons studied displayed polysynaptic inhibitory responses. It could be that this result was due to the high threshold for action potential activation in the interneuron intercalated between the callosal fibers and the recorded cell. This proved to be the case in some pyramidal cells but not in interneurons, in which, on the other hand, spontaneous IPSCs were detectable. Therefore, we believe that the lack of feedforward inhibition observed in some pyramidal cells and in all interneurons represents a genuine feature. The axon of interneurons studied generally branched mainly within the layer where the cell body was located in a typical basket cell pattern, and it is thus, likely that only the interneurons located in layer VI, and not in layer V, provided feedforward inhibition to the few layer VI pyramidal cells that showed it. In contrast to our data, polysynaptic IPSPs have been reported in layer II/III and V pyramidal cells after stimulation of the corpus callosum in vitro (Vogt and Gorman 1982; Thomson 1986; Kawaguchi 1992; Conti and Manzoni 1994) and in vivo (Toyama and others 1974; Conti and Manzoni 1994; Cisse and others 2003). The absence of feedforward inhibition is likely to facilitate excitation between neurons of the 2 hemispheres and also to result in an increase of the time window for EPSPs summation.

Functional Implication of the Present Results for the Cortical Microcircuits Activated by the Corpus Callosum

It has been previously documented that pyramidal neurons receiving inputs from the corpus callosum are located in cortical layers II/III and V and that the callosal projection terminates exclusively with excitatory synapses on spines of pyramidal neurons of the contralateral cortex (Akers and Killackey 1978; Cipolloni and Peters 1983) and rarely on dendritic shafts or cell bodies. However, our data together with others (Carr and Sesack 1998; Cisse and others 2003) challenge this view. We show here that PV-positive GABAergic interneurons of deep cortical layers of RSA/frontal cortex receive synapses on dendrites and somata and are directly activated by the contralateral hemisphere. The functional involvement of interneurons in the callosal-cortical network can be appreciated at integrative level by the finding that the receptive fields of neurons in the primary somatosensory cortex of monkey, which are subjected to the influence of GABAergic inhibition, are widened when the activity of the contralateral hemisphere is dampen down (Clarey and others 1996). More recently, it was postulated that the excitatory drive of the contralateral hemisphere onto layer IV interneurons alters the receptive field of somatosensory columns (Pluto and others 2005). Furthermore, our finding that GABAergic interneurons are directly excited by commissural fibers may provide a cellular substrate to the clinical observation of transcallosal inhibition, which is reduced by stroke (Pascual-Leone and others 2005).

We also found that pyramidal neurons of layer VI are monosynaptically excited by the callosal fibers. This finding also fills a gap in literature because these neurons were clearly different from the pyramidal neurons of layers II/III and V that have a large soma and are the classical target of callosal fibers. We show here that layer VI also contains putative excitatory type I synapses formed by callosal axon terminals, in agreement with previous reports (Vogt and others 1981; White and Czeiger 1991). The pyramidal cells studied here had a relatively small soma and an apical dendrite oriented toward either deep or superficial cortical layers, consistent with previous studies. Our upright pyramidal neurons could be corticothalamic cells (Brumberg and others 2003), whereas the inverted pyramids could be corticocortical neurons sending axonal arbors ipsi- or contralaterally (Zhang and Deschenes 1997, 1998; Prieto and Winer 1999), with the latter rarely contacting interneurons (Mercer and others 2005). Therefore, the information conveyed by the callosal fibers would then spread from layer VI neurons toward the thalamus synchronizing a bilateral cortical-thalamic loop, as well as toward several other cortical sites.

Although most callosal fibers are excitatory, anatomical studies have shown that during the early stages of development, 21% of them arise from GABAergic cells (Elberger 1994; Riederer and others 2004), and this value becomes smaller after reaching adulthood, falling to 0.7–5% (Gonchar and others 1995; Fabri and Manzoni 2004). Consistent with this data, all the retrogradely labeled neurons we recorded from P22–P24 rats were either upright or inverted pyramidal cells. At least 3 different not mutually exclusive models of cellular interhemispheric connectivity have been proposed (Innocenti 1986): callosal neurons projecting to noncallosal neurons (heterologous model), callosal neurons interconnected but not reciprocally (homologous model), callosal neurons reciprocally interconnected (reciprocal model). Our data support the homologous model, and possibly the reciprocal model, because callosal stimulation evoked monosynaptic EPSCs in the retrogradely labeled neurons tested. This result, together with the lack of feedforward inhibition we observed, would facilitate point-to-point fast excitation between layer VI pyramidal neurons placed at homologous areas of the 2 hemispheres leading to synchronization of cerebral activity (Engel and others 1991).

Notes

This work was supported by the Medical Research Council, UK. We thank Prof Peter Somogyi for help with immunocytochemistry and microscopy and together with Drs Zoltan Molnar and Ole Paulsen for critical suggestions on a previous version of the manuscript. We also thank Prof Paul Bolam, Dr Justin Boyes, Romana Hauer, Dr Juan Mena-Segovia, Ben Micklem, Liz Norman, David Roberts, and Wai Yee Suen for technical aid and expertise and Prof M. Watanabe for providing the VGAT antibody. *Conflict of Interest*: None declared.

Address correspondence to Dr Marco Capogna, MRC Anatomical Neuropharmacology Unit, Mansfield Road, Oxford OX1 3TH, UK. marco.capogna@pharm.ox.ac.uk.

References

Akers RM, Killackey HP. 1978. Organization of corticocortical connections in the parietal cortex of the rat. J Comp Neurol 181:513–537.

Angulo MC, Staiger JF, Rossier J, Audinat E. 1999. Developmental synaptic changes increase the range of integrative capabilities of an identified excitatory neocortical connection. J Neurosci 19:1566–1576.

Beierlein M, Connors BW. 2002. Short-term dynamics of thalamocortical and intracortical synapses onto layer 6 neurons in neocortex. J Neurophysiol 88:1924–1932.

Berlucchi G, Aglioti S, Marzi CA, Tassinari G. 1995. Corpus callosum and simple visuomotor integration. Neuropsychologia 33:923–936.

Bogen JE. 1986. Mental duality in the intact brain. Bull Clin Neurosci 51:3–29.

Brumberg JC, Hamzei-Sichani F, Yuste R. 2003. Morphological and physiological characterization of layer VI corticofugal neurons of mouse primary visual cortex. J Neurophysiol 89:2854–2867.

Buzsaki G. 1984. Feed-forward inhibition in the hippocampal formation. Prog Neurobiol 22:131–153.

Carr DB, Sesack SR. 1998. Callosal terminals in the rat prefrontal cortex: synaptic targets and association with GABA-immunoreactive structures. Synapse 29:193–205.

Celio MR. 1986. Parvalbumin in most gamma-aminobutyric acid-containing neurons of the rat cerebral cortex. Science 231:995–997.

Cipolloni PB, Peters A. 1983. The termination of callosal fibres in the auditory cortex of the rat. A combined Golgi-electron microscope and degeneration study. J Neurocytol 12:713–726.

Cisse Y, Crochet S, Timofeev I, Steriade M. 2004. Synaptic enhancement induced through callosal pathways in cat association cortex. J Neurophysiol 92:3221–3232.

Cisse Y, Grenier F, Timofeev I, Steriade M. 2003. Electrophysiological properties and input-output organization of callosal neurons in cat association cortex. J Neurophysiol 89:1402–1413.

Clarey JC, Tweedale R, Calford MB. 1996. Interhemispheric modulation of somatosensory receptive fields: evidence for plasticity in primary somatosensory cortex. Cereb Cortex 6:196–206.

Conti F, Manzoni T. 1994. The neurotransmitters and postsynaptic actions of callosally projecting neurons. Behav Brain Res 64:37–53.

Devinsky O, Laff R. 2003. Callosal lesions and behavior: history and modern concepts. Epilepsy Behav 4:607–617.

Doyle MW, Andresen MC. 2001. Reliability of monosynaptic sensory transmission in brain stem neurons in vitro. J Neurophysiol 85:2213–2223.

Elberger AJ. 1994. The corpus callosum provides a massive transitory input to the visual cortex of cat and rat during early postnatal development. Behav Brain Res 64:15–33.

Engel AK, Konig P, Kreiter AK, Singer W. 1991. Interhemispheric synchronization of oscillatory neuronal responses in cat visual cortex. Science 252:1177–1179.

Fabri M, Manzoni T. 2004. Glutamic acid decarboxylase immunoreactivity in callosal projecting neurons of cat and rat somatic sensory areas. Neuroscience 123:557–566.

Fabri M, Polonara G, Del Pesce M, Quattrini A, Salvolini U, Manzoni T. 2001. Posterior corpus callosum and interhemispheric transfer of somatosensory information: an fMRI and neuropsychological study of a partially callosotomized patient. J Cogn Neurosci 13: 1071–1079.

Fagiolini M, Fritschy JM, Low K, Mohler H, Rudolph U, Hensch TK. 2004. Specific GABAA circuits for visual cortical plasticity. Science 303:1681–1683.

Gabernet L, Jadhav SP, Feldman DE, Carandini M, Scanziani M. 2005. Somatosensory integration controlled by dynamic thalamocortical feed-forward inhibition. Neuron 48:315–327.

Gazzaniga MS. 2005. Forty-five years of split-brain research and still going strong. Nat Rev Neurosci 6:653–659.

Geiger JR, Lubke J, Roth A, Frotscher M, Jonas P. 1997. Submillisecond AMPA receptor-mediated signaling at a principal neuron-interneuron synapse. Neuron 18:1009–1023.

Gonchar YA, Johnson PB, Weinberg RJ. 1995. GABA-immunopositive neurons in rat neocortex with contralateral projections to S-I. Brain Res 697:27–34.

Hestrin S. 1993. Different glutamate receptor channels mediate fast excitatory synaptic currents in inhibitory and excitatory cortical neurons. Neuron 11:1083–1091.

Hicks TP, Guedes RC. 1983. Neuropharmacological properties of electrophysiologically identified, visually responsive neurones of the posterior lateral suprasylvian area. A microiontophoretic study. Exp Brain Res 49:157–173.

Innocenti GM. 1986. General organisation of callosal connections in the cerebral cortex. In: Jones EG and Peters A editors. Cerebral cortex. Sensory-motor areas and aspects of cortical connectivity. New York: Plenum. p 291–353.
Jonas P. 2000. The time course of signaling at central glutamatergic synapses. News Physiol Sci 15:83–89.
Jonas P, Major G, Sakmann B. 1993. Quantal components of unitary EPSCs at the mossy fibre synapse on CA3 pyramidal cells of rat hippocampus. J Physiol 472:615–663.
Katz LC, Iarovici DM. 1990. Green fluorescent latex microspheres: a new retrograde tracer. Neuroscience 34:511–520.
Kawaguchi Y. 1992. Receptor subtypes involved in callosally-induced postsynaptic potentials in rat frontal agranular cortex in vitro. Exp Brain Res 88:33–40.
Kawaguchi Y, Kubota Y. 1997. GABAergic cell subtypes and their synaptic connections in rat frontal cortex. Cereb Cortex 7:476–486.
Kimura F, Baughman RW. 1997. GABAergic transcallosal neurons in developing rat neocortex. Eur J Neurosci 9:1137–1143.
Kumar SS, Bacci A, Kharazia V, Huguenard JR. 2002. A developmental switch of AMPA receptor subunits in neocortical pyramidal neurons. J Neurosci 22:3005–3015.
Kumar SS, Huguenard JR. 2001. Properties of excitatory synaptic connections mediated by the corpus callosum in the developing rat neocortex. J Neurophysiol 86:2973–2985.
Kumar SS, Huguenard JR. 2003. Pathway-specific differences in subunit composition of synaptic NMDA receptors on pyramidal neurons in neocortex. J Neurosci 23:10074–10083.
Markram H, Toledo-Rodriguez M, Wang Y, Gupta A, Silberberg G, Wu C. 2004. Interneurons of the neocortical inhibitory system. Nat Rev Neurosci 5:793–807.
Mercer A, West DC, Morris OT, Kirchhecker S, Kerkhoff JE, Thomson AM. 2005. Excitatory connections made by presynaptic cortico-cortical pyramidal cells in layer 6 of the neocortex. Cereb Cortex.
Mori M, Abegg MH, Gahwiler BH, Gerber U. 2004. A frequency-dependent switch from inhibition to excitation in a hippocampal unitary circuit. Nature 431:453–456.
Nyiri G, Stephenson FA, Freund TF, Somogyi P. 2003. Large variability in synaptic N-methyl-D-aspartate receptor density on interneurons and a comparison with pyramidal-cell spines in the rat hippocampus. Neuroscience 119:347–363.
Pascual-Leone A, Amedi A, Fregni F, Merabet LB. 2005. The plastic human brain cortex. Annu Rev Neurosci 28:377–401.
Paxinos G, Watson C. 1982. The rat brain in stereotaxic coordinates. Australia: Academic Press.
Pluto CP, Chiaia NL, Rhoades RW, Lane RD. 2005. Reducing contralateral SI activity reveals hindlimb receptive fields in the SI forelimb-stump representation of neonatally amputated rats. J Neurophysiol 94:1727–1732.
Povysheva NV, Gonzalez-Burgos G, Zaitsev AV, Kroner S, Barrionuevo G, Lewis DA, Krimer LS. 2006. Properties of excitatory synaptic responses in fast-spiking interneurons and pyramidal cells from monkey and rat prefrontal cortex. Cereb Cortex 16:541–552.
Prieto JJ, Winer JA. 1999. Layer VI in cat primary auditory cortex: Golgi study and sublaminar origins of projection neurons. J Comp Neurol 404:332–358.
Rao SG, Williams GV, Goldman-Rakic PS. 2000. Destruction and creation of spatial tuning by disinhibition: GABA(A) blockade of prefrontal cortical neurons engaged by working memory. J Neurosci 20:485–494.
Riederer BM, Berbel P, Innocenti GM. 2004. Neurons in the corpus callosum of the cat during postnatal development. Eur J Neurosci 19:2039–2046.
Sah P, Hestrin S, Nicoll RA. 1990. Properties of excitatory postsynaptic currents recorded in vitro from rat hippocampal interneurones. J Physiol 430:605–616.
Swadlow HA. 2003. Fast-spike interneurons and feedforward inhibition in awake sensory neocortex. Cereb Cortex 13:25–32.
Temereanca S, Simons DJ. 2004. Functional topography of cortico-thalamic feedback enhances thalamic spatial response tuning in the somatosensory whisker/barrel system. Neuron 41:639–651.
Thomson AM. 1986. A magnesium-sensitive post-synaptic potential in rat cerebral cortex resembles neuronal responses to N-methylaspartate. J Physiol 370:531–549.
Thomson AM, Bannister AP. 2003. Interlaminar connections in the neocortex. Cereb Cortex 13:5–14.
Toyama K, Matsunami K, Ono T, Tokashiki S. 1974. An intracellular study of neuronal organization in the visual cortex. Exp Brain Res 21:45–66.
Tsay D, Yuste R. 2004. On the electrical function of dendritic spines. Trends Neurosci 27:77–83.
van Brederode JF, Snyder GL. 1992. A comparison of the electrophysiological properties of morphologically identified cells in layers 5B and 6 of the rat neocortex. Neuroscience 50:315–337.
Vogt BA, Gorman AL. 1982. Responses of cortical neurons to stimulation of corpus callosum in vitro. J Neurophysiol 48:1257–1273.
Vogt BA, Rosene DL, Peters A. 1981. Synaptic termination of thalamic and callosal afferents in cingulate cortex of the rat. J Comp Neurol 201:265–283.
West DC, Mercer A, Kirchhecker S, Morris OT, Thomson AM. 2006. Layer 6 cortico-thalamic pyramidal cells preferentially innervate interneurons and generate facilitating EPSPs. Cereb Cortex 16:200–211.
White EL, Czeiger D. 1991. Synapses made by axons of callosal projection neurons in mouse somatosensory cortex: emphasis on intrinsic connections. J Comp Neurol 303:233–244.
Zhang ZW, Deschenes M. 1997. Intracortical axonal projections of lamina VI cells of the primary somatosensory cortex in the rat: a single-cell labeling study. J Neurosci 17:6365–6379.
Zhang ZW, Deschenes M. 1998. Projections to layer VI of the posteromedial barrel field in the rat: a reappraisal of the role of cortico-thalamic pathways. Cereb Cortex 8:428–436.